Molecular Assembly Lines in Active Droplets

Tyler S. Harmon[1,2,3,*] and Frank Jülicher[1,4,5,†]

[1]Max Planck Institute for the Physics of Complex Systems, Nöthnitzerstraße 38, 01187 Dresden, Germany
[2]Max Planck Institute of Molecular Cell Biology and Genetics, Pfotenhauerstraße 108, 01307 Dresden, Germany
[3]Leibniz-Institut für Polymerforschung Dresden e.V., Hohestraße 6, 01069 Dresden, Germany
[4]Center for Systems Biology Dresden, 01307 Dresden, Germany
[5]Cluster of Excellence Physics of Life, TU Dresden, 01062 Dresden, Germany

(Received 24 June 2020; revised 30 November 2021; accepted 21 January 2022; published 9 March 2022)

Large protein complexes are assembled from protein subunits to form a specific structure. In our theoretic work, we propose that assembly into the correct structure could be reliably achieved through an assembly line with a specific sequence of assembly steps. Using droplet interfaces to position compartment boundaries, we show that an assembly line can be self-organized by active droplets. As a consequence, assembly steps can be arranged spatially so that a specific order of assembly is achieved and incorrect assembly is strongly suppressed.

DOI: 10.1103/PhysRevLett.128.108102

Large complexes play important roles in several critical aspects of life. Examples are bacterial flagellar motors, viral capsids, proteasomes, and ribosomes. Many of such complexes must be assembled into a specific arrangement in order to function. An important question is how such complexes can be created at high efficiency and fast rate, avoiding the formation of incorrect and incomplete assemblies [1–15]. One strategy of self-assembly is complex formation through a thermodynamic process where the assembled state is a free energy minimum [2,3]. There could exist several accessible minima such that self-assembly would not lead to a unique structure or that it is slowed by trapping in metastable intermediates [1–3,11].

Alternative strategies based on nonequilibrium assembly could avoid the problems of thermodynamic self-assembly or allow for the assembly of structures that cannot be reached by minimizing the free energy [1,11,14]. This can be achieved when components assemble in a specific temporal order. One such strategy uses sequential synthesis to provide subunits when specific assembly phases have completed. Incorrect binding of subunits is prevented by allowing them to encounter the nascent complex when only the correct binding site is accessible, which limits the assembly rate. This strategy is employed, for example, in the assembly of the bacterial flagella motor [16].

Examples of nonequilibrium assembly lead us to the question of whether complex assembly could emerge via nonequilibrium patterns in a self-organized process. More precisely, we ask whether reliable and rapid assembly of complexes with a specific structure can be achieved in steady state where components flow in and complexes flow out. We show that this is possible in a self-organized assembly line. The assembly line organizes assembly steps in space, thereby providing a specific temporal order during complex assembly. Such assembly lines could be organized within biochemical compartments.

Biochemical compartments in cells either have a membrane or are membraneless. Membraneless compartments are often liquidlike biomolecular condensates that can be described as droplets that result from phase coexistence with their surroundings [17–20]. A rich diversity of geometries for coexisting droplets has been observed in cells. One example is a smaller droplet inside a larger droplet [21,22]. It remains an open question of what functions such an arrangement of compartments can have. Here, we propose such arrangements can play a role to organize assembly lines in cells.

Here, we present the theory of nonequilibrium complex formation by a self-organized assembly line. These emerge as patterns in reaction-diffusion systems that are confined in droplets. These patterns consist of separated bands of distinct reactions which correspond to different assembly steps. Chemical patterns are typically viewed through the lens of patterns of concentrations, whereas these bands reflect the localization of distinct reactions while the molecular species are not localized. The spatial arrangement of different assembly steps defines the temporal order in which subunits are added to the complex. This process can occur at steady state with a constant influx of subunits and constant outflux of finished complexes. This scenario allows rapid and accurate assembly.

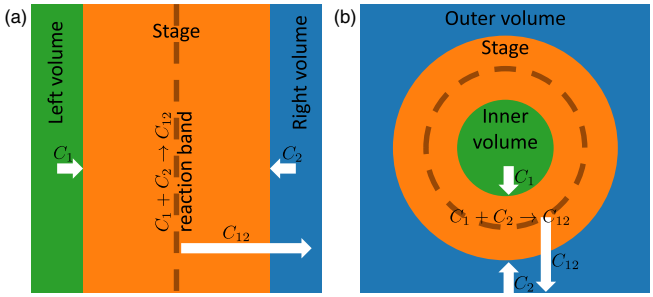

FIG. 1. Spatial organization of macromolecular assembly. (a) 1D arrangement of compartments for molecular assembly. Component C_1 is produced in the left volume (green) and component C_2 is produced in the right volume (blue). Assembly of the complex C_{12} occurs in the stage volume (orange). Assembly can be localized to a band between the left and right volumes (dashed line). The complex is exported via the right volume. (b) 3D arrangement of compartments for molecular assembly. Component C_1 is produced in the inner volume (green) and component C_2 is produced in the outer volume (blue). Assembly of the complex C_{12} occurs in the stage volume (orange). Assembly can be localized to a spherical band between the inner and outer volumes (dashed line). The complex is exported via the outer volume.

First, we examine a minimal model in one dimension where molecular assembly steps can be positioned along a line and separated in space. The region $[0, L]$ corresponds to the stage where assembly steps occur. The left boundary connects the stage to the inner volume, and the right boundary connects the stage to the outer volume which serve as reservoirs that provide components, see Fig. 1(a). We consider two components C_1 and C_2, which enter from the left and right boundaries, respectively. These components bind irreversibly to form a complex, $C_1 + C_2 \to C_{12}$ which leaves via the outer volume. All molecular species move by diffusion and associate following mass action kinetics. The system is thus described by the association diffusion equations along the position coordinate x given by

$$\frac{\partial}{\partial t} n_1 = D \frac{\partial^2}{\partial x^2} n_1 - k n_1 n_2, \tag{1a}$$

$$\frac{\partial}{\partial t} n_2 = D \frac{\partial^2}{\partial x^2} n_2 - k n_1 n_2, \tag{1b}$$

where n_1 and n_2 are the concentrations of components C_1 and C_2, respectively, and D and k are the diffusion constant and association rate. For simplicity we have chosen equal diffusivities. These equations are complemented by boundary conditions that connect the stage to the inner and outer volumes. We consider the case where there are no sinks in the inner volume and C_1 and C_2 are produced only in the inner and outer volumes, respectively. Accordingly, we impose a constant influx J of component C_1 and no flux of component C_2 at $x = 0$. At $x = L$ we impose boundary conditions that depend on the concentrations n_1 and n_2 which describes partitioning of molecules between the stage and the outer volume. The boundary conditions thus read

$$D \partial_x n_1|_{x=0} = -J, \tag{2a}$$

$$D \partial_x n_2|_{x=0} = 0, \tag{2b}$$

$$D \partial_x n_1|_{x=L} = -\beta n_1(x = L), \tag{2c}$$

$$D \partial_x n_2|_{x=L} = \alpha - \beta n_2(x = L). \tag{2d}$$

Here, α corresponds to the source of C_2 and β corresponds to sinks of C_1 and C_2.

Of particular interest to us is the steady state solution for the concentrations and the profile of the association flux $\Phi \equiv k n_1 n_2$ as a function of x. In Fig. 2(a) we show examples of stationary profiles of the association flux that reveal the localization of the association to different positions x_M depending on the magnitude of α, the source of C_2. Figure 2(b) shows the corresponding steady state concentration profiles.

Away from the region of high association flux, the fluxes for the two components are equal and opposite because assembly consumes an equal number of both components. As a result, Eq. (1) has symmetric solutions with respect to x_M if the boundaries are far from the assembly volume. In this limiting case, assembly is fully efficient within $x = [0, L]$, and we can calculate the exact position x_M and approximate the variance σ^2 of the association flux profile, see Supplemental Material [23],

$$x_M = L - D \frac{\alpha - J}{J\beta}, \tag{3}$$

$$\sigma \approx \sqrt{\frac{2}{\pi}} \left(1 + \frac{\pi}{2} + \sqrt{1 + \pi}\right)^{1/3} \left(\frac{D^2}{kJ}\right)^{1/3}. \tag{4}$$

The limit where boundaries are far from the assembly volumes corresponds to $\sigma \ll x_m$ and $\sigma \ll L - x_m$.

This result shows that assembly steps can be localized to regions of width σ centered at position x_M. This localization of assembly steps can be used to generate assembly lines. Assembly is initiated by a molecule that enters the stage from the left. It first encounters a single component from the right boundary to which it can bind. As the assembling complex diffuses toward the right, it will encounter sequentially additional components that arrive from the right boundary. In this assembly line, the complex grows as it diffuses toward the right boundary. These components can thus be incorporated in a prescribed order to ensure correct assembly. This is schematically represented in Fig. 2(c). Assembly regions can be arranged in space such that they are separated by more than a distance σ. This implies that the addition of one type of component is completed before the complex encounters the next component. The spatial order of assembly regions specifies the

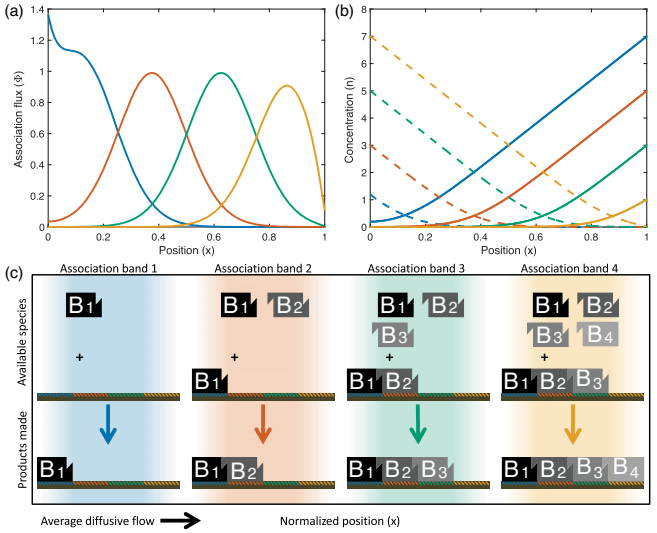

FIG. 2. Positioning of assembly steps in narrow regions. (a) Normalized assembly flux Φ as a function of normalized position x in the stage region for different values of the normalized influx α of component C_2 [$\alpha = 70$ (blue), 50 (orange), 30 (green), 10 (yellow)]. (b) Steady state concentrations of components C_1 (dashed) and C_2 (solid) for the same values of α as in (a). Shown are numerical solutions of the minimal model given by Eqs. (2) and (3). (c) Cartoon schematic of how an assembly line could be organized. The foundation molecule tends to diffuse to the right progressing through the different association bands. Progressing to each sequential association bands adds another available brick that can bind to the foundation. Parameter values are $J = 0.31$, $D = 0.039$, $k = 5.9$, $\beta = 10$, and $L = 1$.

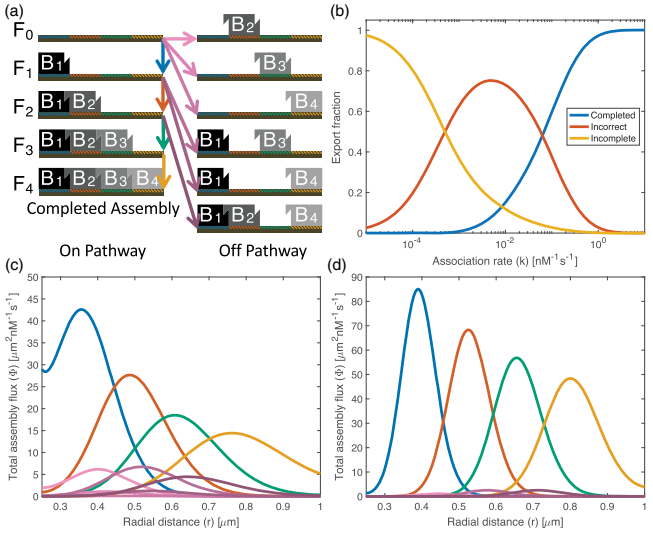

FIG. 3. Self-organized molecular assembly lines. (a) Scheme of the on pathway assembly steps (blue, red, green, and yellow arrows) and off-pathway dead ends (pink arrows). Here, F_0 represents the foundation and B_1, B_2, B_3, B_4 represent the bricks. The on-pathway intermediates are denoted F_1, F_2, F_3, and F_4 is the correctly assembled product. (b) Fraction of completed (green), incomplete (yellow), and incorrect (red) assemblies that leave the stage in steady state as a function of the association rate k. (c) Radial profiles of total assembly fluxes $\Phi = 4\pi r^2 k n_{F,i} n_{B,j}$ at steady state for the four on-pathway associations (blue, red, green, yellow) and the off-pathway associations (pink) for association rate $k = 0.038\ \mathrm{nM^{-1}\,s^{-1}}$. Here, $n_{F,i}$ and $n_{B,j}$ are concentrations of associating components. (d) same as (c) but for $k = 0.27\ \mathrm{nM^{-1}\,s^{-1}}$. The curves shown in (c) and (d) correspond to the assembly steps shown in (a) in the same color. Shown in (b)–(d) are numerical solutions for spherical geometry and parameter values $J = 10\mu\mathrm{m^3\,nM\,s^{-1}}$, $\beta_F = 1.26\ \mu\mathrm{m^3\,s^{-1}}$, $\beta_B = 1.26\ \mu\mathrm{m^3\,s^{-1}}$, $r_1 = 0.25\ \mu$m, $r_2 = 1.0\ \mu$m, $D_F = 0.01\ \mu\mathrm{m^2\,s^{-1}}$, $D_{B,i} = 0.01\ \mu\mathrm{m^2\,s^{-1}}$, and $\alpha_{B,i} = (138, 82, 50, 29)\ \mu\mathrm{m^3\,nM\,s^{-1}}$ for $i = (1, 2, 3, 4)$.

dominant temporal order of assembly steps. This assembly line can operate at steady state with all assembly steps being conducted concurrently.

We now discuss an example of how such an assembly line could be realized in three dimensions using concentric spherical droplets where a small droplet is located in the center of a larger droplet, see Fig. 1(b). The foundational component, denoted F_0, is produced inside the small central droplet which defines the inner volume. In our example, we consider four assembly bricks, B_i, $i = 1, \ldots, 4$, which are provided in the outer volume that surrounds both droplets. The stage volume is the space in the larger droplet between the inner volume and outer volume. The foundation and bricks enter the stage from opposite sides.

To highlight the impact of the assembly line we model both desirable and undesirable associations. We call the intermediate assemblies assembled in the correct sequential order the on-pathway intermediates, denoted by F_i, where i is the index of the last brick that was incorporated into the complex. In this logic, F_4 is the correctly assembled final complex. If binding occurs in a different order then complex formation is unsuccessful and is called off pathway. Figure 3(a) shows a schematic of all constructs and associations, both on and off pathway. Inside the stage the concentration fields are described by association-diffusion equations that capture the diffusion of components and their association steps,

$$\frac{\partial}{\partial t} n_{F,i} = D_{F,i} \nabla^2 n_{F,i} - k n_{F,i} n_{B,i+1} - k n_{F,i} \Theta(2-i) \sum_{k=i+2}^{4} n_{B,k} + k n_{F,i-1} n_{B,i},$$

$$\frac{\partial}{\partial t} n_{B,i} = D_{B,i} \nabla^2 n_{B,i} - k n_{F,i-1} n_{B,i} - k n_{B,i} \Theta(i-2) \sum_{k=0}^{i-2} n_{F,k}. \tag{5}$$

Here, $n_{B,i}$ is the concentration of brick i, $n_{F,i}$ is the concentration of the free foundation ($i = 0$), the on-pathway intermediates ($i = 1, 2, 3$), and product ($i = 4$). Furthermore D_{F0}, D_{Fi}, and D_{Bi} are the diffusion constants for foundation, complexes, and bricks, respectively, and k is the rate constant for all associations. The Laplace operator is denoted ∇^2 and the Heaviside function is denoted Θ with $\Theta(i) = 1$ if $i \geq 0$ otherwise $\Theta(i) = 0$. These equations are supplemented by boundary conditions at radii r_1 and r_2,

$$\left.\frac{dn_{F,0}}{dr}\right|_{r_1} = -\frac{J}{D_F 4\pi r_1^2}, \tag{6a}$$

$$\left.\frac{dn_{F,i}}{dr}\right|_{r_2} = -\frac{\beta_F n_{F,i}(r_2)}{D_F 4\pi r_2^2}, \tag{6b}$$

$$\left.\frac{dn_{B,i}}{dr}\right|_{r_2} = \frac{\alpha_{B,i} - \beta_{B,i} n_{B,i}(r_2)}{D_{B,i} 4\pi r_2^2}, \tag{6c}$$

where J is the influx of foundation molecules, α_{Bi} is the influx of brick B_i, β_F and $\beta_{B,i}$ describe the concentration dependence of the outflux of the components into the outer volume due to partitioning. Furthermore, we have imposed no flux boundary conditions at r_1 for intermediates F_i where $i \geq 1$ and the bricks B_i. These expressions can be derived for a droplet in a steady state environment.

In spherical coordinates we define the total association flux as

$$\Phi_i = 4\pi r^2 k n_{F,i-1} n_{B,i}. \tag{7}$$

In steady state the total association flux exhibits a maximum at position $r_{M,i}$ with

$$\frac{1}{r_{M,i}} = \frac{1}{r_2} + \frac{4\pi D_{B,i}}{\beta_{B,i}} \left(\frac{\alpha_{B,i} - J}{J}\right), \tag{8}$$

and a width given by

$$\sigma_i \approx 1.33 \left(\frac{4\pi r_{M,i}^2 D_F D_{B,i}}{kJ}\right)^{1/3}, \tag{9}$$

see Supplemental Material [23]. Figure 3(b) shows the fraction of complete, incomplete, and incorrect assemblies leaving the stage at steady state as a function of association rate. The fraction of complete assemblies defines the efficiency of the system. Figures 3(c) and 3(d) show the radial profiles of the total association fluxes for two different association rates. The association rate primarily changes the width of the peaks of the total association flux but not the position, see Eqs. (8) and (9). For more sharply peaked total association fluxes, the efficiency of assembly is higher because different assembly steps are better separated in space. Accordingly, assembly efficiency increases as the association rate increases and off-pathway associations are highly suppressed, see Fig. 3(b). The general requirement for assembly lines to improve assembly efficiency is that the spacing between association bands is larger than the width of the bands.

We have shown that molecular assembly lines could be self-organized in phase separated condensates. Such an assembly line requires a spatial organization of association steps which distinguishes it from well mixed association scenarios. This spatial organization can lead to a high-throughput assembly by operating at steady state. Additionally, efficient assembly can be achieved through controlling the temporal order in which subunits are added via the spatial separation of the assembly bands. The scenario proposed here has four hallmarks that could be seen in experiments: (i) association but not concentration is confined to distinct spatial bands, (ii) unbound components can be found close to their source but not past the position where they are added to the complex, (iii) the average complex size increases toward the outer boundary, and (iv) changing the concentration ratio of components yields incomplete or incorrectly assembled complexes because assembly bands can become rearranged.

We considered simplified geometries in one and three dimensions, motivated by liquidlike condensates. However, the strategy discussed here is more general and can also work in other geometries. As illustrated in the one dimensional case, the assembly steps are positioned at specific distances from the outer surface. Therefore, our work suggests that in nonspherical geometries, assembly steps are positioned to nonintersecting manifolds inside the outer surface. We expect this mechanism to robustly self-organize assembly lines in three dimensions in a broader collection of geometries, including multiple inner volumes.

Comparing self-organized assembly lines described here to assemble under well mixed conditions reveals the benefits of assembly lines. Efficient assembly under well mixed conditions requires larger amounts of unfinished complexes to achieve the same export rate, see Supplemental Material [23].

An important question is whether the simple arguments presented here still apply when molecular noise is taken into account. We have performed stochastic simulations of the noisy association-diffusion system and find that distinct assembly bands emerge in the presence of noise even at relatively low rates of molecular influx, see Supplemental Material [23].

In principle, complexes can also form without a fixed temporal order. For example, the time order is irrelevant if there are many identical components as in the case of viral capsids. On the other extreme, if all components are different then temporal order can be helpful. In this case it is likely that several local minima exist which correspond to different assembled structures. In principle a unique structure emerges as the lowest energy configuration but

this may take a long time. However, if the temporal order is controlled, a specific local minimum could be consistently reached. Therefore, time ordered assembly provides a strategy to reliably assemble many components into a specific structure. For simplicity we have considered irreversible assembly steps. In practice molecular binding events are reversible and the limit of irreversible steps corresponds to a situation where the time scale for an unbinding event is slower than the time between subsequent assembly steps, see Supplemental Material [23].

For simplicity the above sections focused on the case where bricks are added one at a time. An interesting situation arises when several components form a small complex that then associates with the nascent assembly. In the supplement we show that one can map this model on the original framework where the brick represents the complex instead of the constituent components.

An important example of molecular assembly are RNA-protein complexes. The components of such complexes can fit well into our simplified assembly scheme, shown in Fig. 3(a). Here, bricks (proteins) are added to a foundational element (RNA) and are supplied from different regions (translation in the cytoplasm and transcription in the nucleus, respectively).

The most prominent example of an RNA-protein complex is the ribosome which mainly consists of large RNA and many different small proteins [29–31]. Ribosomes are assembled in the nucleolus, a liquidlike droplet-inside-droplet compartment in the cell nucleus. Ribosomal RNA is produced in the inner compartment of the nucleolus called the dense fibrillar component, corresponding to the inner volume. Ribosomal proteins are provided in the nucleoplasm, corresponding to the outer volume. The assembly occurs in the granular component of the nucleolus corresponding to the stage volume. Given this arrangement, ribosome assembly is an ideal candidate for the molecular assembly line proposed here. In the supplement we discuss parameter values, in particular those relevant to condensates found inside cells. This motivates the parameter values used in Fig. 3 and shows that an assembly line can self-organize for parameter values accessible to cells. It will be interesting to explore whether signatures of an assembly line can be found here. An interesting question is whether assembly bands could be directly observed experimentally. This poses a challenge because labeling components alone may not reveal the spatial organization of an assembly line. This is because fluorescent labels would be attached to a component as well as to the assembled complex. Even if the assembly is organized into distinct bands, the fluorescent signal would not show this structure. Techniques such as FRET could differentiate between bound and unbound components and thus are promising to reveal spatial patterns of assembly processes.

In addition to the nucleolus, other liquidlike compartments could play a role to organize the assembly of macromolecular complexes. An example is *p* granules in *C. elegans* which can be located on the nuclear membrane and cover nuclear pores [32]. This setting has the important feature that *p* granules can communicate with two different compartments at the same time, the cytoplasm and nucleoplasm, allowing opposing fluxes from both compartments. This suggests that *p* granules are also naturally suited for reliable molecular processing using assembly lines of the type proposed here. More generally, liquidlike compartments are expected to self-organize biochemical processes in space. Our work therefore provides new insights into the possible role of liquidlike condensates for biological processes.

We thank Rabea Seyboldt, Anthony A. Hyman, Richard W. Kriwacki, and Diana Mitrea for useful discussions. F. J. acknowledges funding by the Volkswagen foundation.

*tylerharmon@pks.mpg.de
†julicher@pks.mpg.de

[1] F. M. Gartner, I. R. Graf, P. Wilke, P. M. Geiger, and E. Frey, eLife **9**, 1 (2020).
[2] J. Grant, R. L. Jack, and S. Whitelam, J. Chem. Phys. **135** (2011).
[3] M. F. Hagan, O. M. Elrad, and R. L. Jack, J. Chem. Phys. **135** (2011).
[4] C. Chen, C. C. Kao, and B. Dragnea, J. Phys. Chem. A **112**, 9405 (2008).
[5] M. F. Hagan and O. M. Elrad, Biophys. J. **98**, 1065 (2010).
[6] G. R. Lazaro and M. F. Hagan, J. Phys. Chem. B **120**, 6306 (2016).
[7] A. Reinhardt and D. Frenkel, Phys. Rev. Lett. **112**, 238103 (2014).
[8] W. M. Jacobs, A. Reinhardt, and D. Frenkel, Proc. Natl. Acad. Sci. U.S.A. **112**, 6313 (2015).
[9] Y. Ke, L. L. Ong, W. M. Shih, and P. Yin, Science **338**, 1177 (2012).
[10] W. M. Jacobs and D. Frenkel, Soft Matter **11**, 8930 (2015).
[11] S. Whitelam, Soft Matter **11**, 8225 (2015).
[12] R. P. Sear, J. Phys. Condens. Matter **19**, 033101 (2007).
[13] B. Wei, M. Dai, and P. Yin, Nature (London) **485**, 623 (2012).
[14] G. M. Rotskoff and P. L. Geissler, Proc. Natl. Acad. Sci. U.S.A. **115**, 6341 (2018).
[15] B. Chen, Biochemistry **55**, 2539 (2016).
[16] U. Alon, in *An Introduction to Systems Biology: Design Principles of Biological Circuits* (CRC Press, Boca Raton, 2006), Chap. 5, pp. 75–92.
[17] P. Li, S. Banjade, H. C. Cheng, S. Kim, B. Chen, L. Guo, M. Llaguno, J. V. Hollingsworth, D. S. King, S. F. Banani *et al.*, Nature (London) **483**, 336 (2012).
[18] S. F. Banani, H. O. Lee, A. A. Hyman, and M. K. Rosen, Nat. Rev. Mol. Cell Biol. **18**, 285 (2017).
[19] P. M. McCall, S. Srivastava, S. L. Perry, D. R. Kovar, M. L. Gardel, and M. V. Tirrell, Biophys. J. **114**, 1636 (2018).
[20] C. A. Weber, D. Zwicker, F. Jülicher, and C. F. Lee, Rep. Prog. Phys. **82** (2019).
[21] M. Feric, N. Vaidya, T. S. Harmon, D. M. Mitrea, L. Zhu, T. M. Richardson, R. W. Kriwacki, R. V. Pappu, and C. P. Brangwynne, Cell **165**, 1686 (2016).

[22] F. M. Boisvert, S. Van Koningsbruggen, J. Navascués, and A. I. Lamond, Nat. Rev. Mol. Cell Biol. **8**, 574 (2007).
[23] See Supplemental Material at http://link.aps.org/supplemental/10.1103/PhysRevLett.128.108102 for detailed derivations, comparisons to assembly without an assembly line, discussions pertaining to additional complexities of the assembly line model, and a discussion about parameters relevant to biology. This includes Refs. [21,24–28].
[24] S. C. Weber and C. P. Brangwynne, Curr. Biol. **25**, 641 (2015).
[25] S. Heyden and M. Ortiz, Comput. Methods Appl. Mech. Eng. **314**, 314 (2017).
[26] A. Huber, S. L. French, H. Tekotte, S. Yerlikaya, M. Stahl, M. P. Perepelkina, M. Tyers, J. Rougemont, A. L. Beyer, and R. Loewith, EMBO J. **30**, 3052 (2011).
[27] L. Jawerth, E. Fischer-Friedrich, S. Saha, J. Wang, T. Franzmann, X. Zhang, J. Sachweh, M. Ruer, M. Ijavi, S. Saha *et al.*, Science **370**, 1317 (2020).
[28] S. H. Northrup and H. P. Erickson, Proc. Natl. Acad. Sci. U.S.A. **89**, 3338 (1992).
[29] H. Tschochner and E. Hurt, Trends Cell Biol. **13**, 255 (2003).
[30] J. H. Davis and J. R. Williamson, Phil. Trans. R. Soc. B **372** (2017).
[31] S. Klinge and J. L. Woolford, Nat. Rev. Mol. Cell Biol. **20**, 116 (2019).
[32] D. L. Updike, S. J. Hachey, J. Kreher, and S. Strome, J. Cell Biol. **192**, 939 (2011).